X-ray Ptychography with a Laboratory Source

Darren J. Batey,[1] Frederic Van Assche,[2] Sander Vanheule,[2] Matthieu N. Boone,[2]
Andrew J. Parnell,[3] Oleksandr O. Mykhaylyk,[4] Christoph Rau,[1] and Silvia Cipiccia[1,5]

[1]*Diamond Light Source, Harwell Science and Innovation Campus, Fermi Avenue, Didcot, UK*

[2]*UGCT-RP, Department of Physics and Astronomy, Ghent University, Belgium*

[3]*Soft Matter Analytical Laboratory, Department of Chemistry, University of Sheffield, Sheffield, UK*

[4]*Department of Physics and Astronomy, University of Sheffield, Sheffield, UK*

[5]*Department of Medical Physics and Biomedical Engineering, University College London, London, UK*

(Dated: February 9, 2021)

Abstract

X-ray ptychography has revolutionised nanoscale phase contrast imaging at large-scale synchrotron sources in recent years. We present here the first successful demonstration of the technique in a small-scale laboratory setting. We conducted an experiment with a liquid metal-jet X-ray source and a single photon-counting detector with a high spectral resolution. The experiment used a spot size of 5 µm to produce a ptychographic phase image of a Siemens star test pattern with a sub-micron spatial resolution. The result and methodology presented show how high-resolution phase contrast imaging can now be performed at small-scale laboratory sources worldwide.

INTRODUCTION

Ptychography is a coherent scanning-diffraction imaging technique that produces quantitative images at resolutions beyond the imaging performance of conventional, lens-based, microscopy systems [1]. Ptychography is now routinely applied at X-ray synchrotron sources across the world, obtaining highly sensitive, quantitative, images at the highest spatial resolutions, down to tens of nanometres [2–7]. Until now, the high level of coherence required for X-ray ptychography has limited the application of the technique to high brilliance sources such as synchrotron and, more recently, FEL facilities [8]. It was recently postulated that the new generation of X-ray laboratory sources may have sufficient brilliance to conduct a ptychographic experiment, given the correct experimental setup [9]. We present here a demonstration of such an experiment and the first proof of concept for far field X-ray ptychography performed using an X-ray laboratory source.

A ptychography scan consists of recording 2D intensity patterns downstream from a sample that is irradiated by a localised spot of coherent radiation. The 4D ptychographic dataset is built up by scanning the sample relative to the beam to a series of overlapping positions. It is possible to record and subsequently invert the data to retrieve the complex refractive index of the object at wavelength limited resolutions across an extended field of view [10–14]. The success of the inversion step in extracting the phase relies strongly on the stability of the instrumentation and coherent properties of the beam. The coherence manifests itself in interference fringes that hold the relative phase information. The coherent fraction of a beam is related to the lateral (i.e. spatial) and longitudinal (i.e. temporal) coherence. The former is determined by the photon energy and the effective source size - how well

confined the source of radiation is laterally in space. The latter is determined by the source bandwidth - how well confined the source of radiation is in wavelength, or longitudinally in space. The level of coherence of an instrument can be described in terms of brilliance. Brilliance is directly proportional to the spatial and temporal coherence. Typical brilliance of third generation light sources is of the order of 10^{20} photons $\mathrm{s}^{-1}\,\mathrm{mm}^{-2}\,\mathrm{mrad}^{-2}$ 0.1% B.W.

In a recent work, we used a detuned synchrotron source and a hyperspectral X-ray detector to demonstrate the feasibility of broadband spectroscopic X-ray ptychography [9]. Due to the specific setup, the brilliance of the synchrotron source was reduced to approximately 3×10^{11} photons $\mathrm{s}^{-1}\,\mathrm{mm}^{-2}\,\mathrm{mrad}^{-2}$ 0.1% B.W. State of the art high brilliance X-ray laboratory sources based on a liquid metal-jet (LMJ) approach this level of brilliance [15]. X-ray ptychography using such a source is therefore feasible, as presented in the following sections.

EXPERIMENT AND RESULTS

Experimental configuration

The experiment was designed and conducted to explore the possibility of ptychographic imaging in a laboratory setting. The data were collected at the University of Sheffield Soft Matter AnalyticaL Laboratory (SMALL) [16, 17], with the portable ptychography endstation from I13-1 of Diamond Light Source and a hyperspectral detector from Ghent University [18, 19]. The X-ray source is an Excillum liquid gallium metal jet (LMJ), which has a brilliance of approximately of 5×10^{11} photons $\mathrm{s}^{-1}\,\mathrm{mm}^{-2}\,\mathrm{mrad}^{-2}$ 0.1% B.W. [15], one order of magnitude higher than conventional microfocus sources [20, 21]. The experimental setup is shown in Figure 1. The spectrum of the source was characterised using the hyperspectral detector and it shows the Gallium (Ga) K-alpha and K-beta lines above the Bremsstrahlung background (see Figure 3 in method section for additional details).

The experiment consisted of a ptychographic scan of a Siemens star test pattern. The ptychographic data was reconstructed through the ePIE operator [12] in PtyREX [22], where the set of intensity measurements are inverted into an image of the object.

The detector made it possible to post-process the data for different bandwidths and exposure times. Two datasets, of bandwidth 200 eV (matching the detector energy resolution at the Ga K-alpha) and 1 keV around the K-alpha line, were generated. The natural spectral

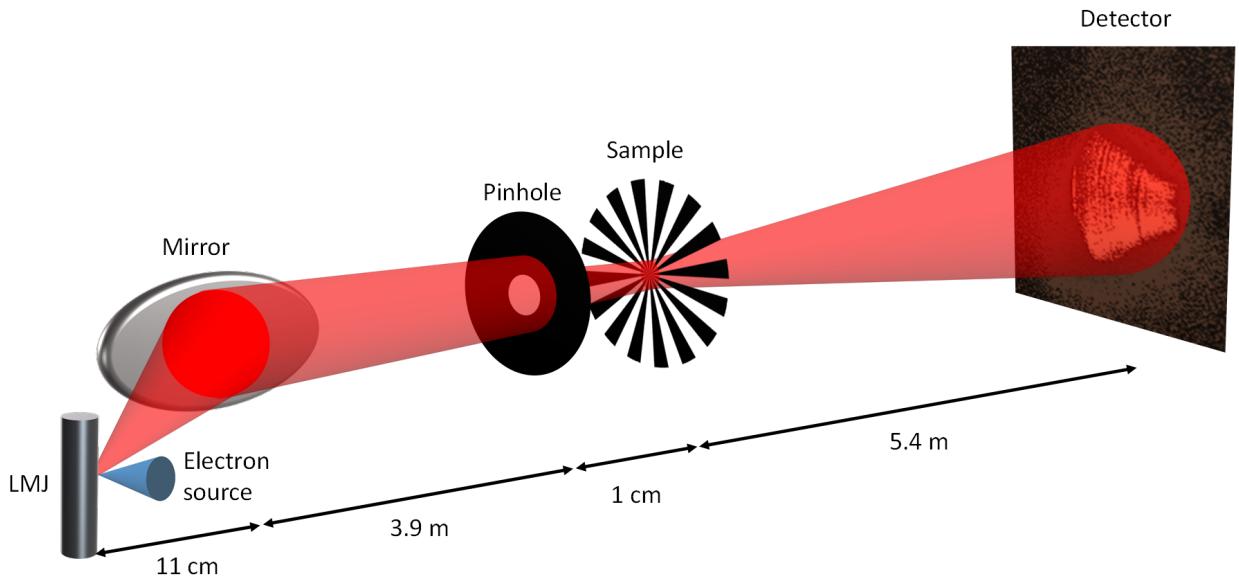

FIG. 1. Experimental configuration. Ptychography setup (not to scale) showing the experimental layout as implemented at SMALL, Sheffield, UK.

width of the K-alpha lines is a few electronvolt, and the distance between K-alpha(1) and K-alpha(2) is 17 eV, hence the recorded bandwidth is determined by the detector energy resolution. Increasing the bandwidth of the data analysed from 200 eV to 1 keV increases the contribution of the Bremsstrahlung background. The theoretical resolution achievable for 200 eV and 1 keV bandwidths are 100 nm and 540 nm respectively [23]. Conversely, the reconstructions of the experimental data showed a decrease in resolution for the narrower bandwidth (1200 nm for 200 eV and 930 nm for 1 keV), suggesting that we are photon limited. The best reconstruction, Figure 2(b), was obtained with 1 keV bandwidth. Both reconstructions included the correction for the source position and direction. These corrections were essential to compensate for long-term instabilities of the source during the acquisition (see method for details). Figure 2(a) confirms a beam profile of 5 µm in extent. A line profile across the reconstructed phase image of the object shows that the spokes are well resolved (Figure 2(c)). The half-bit resolution of the image is 930 nm (Figure 2(d)), a factor of more than 5 beyond the spot size at the sample.

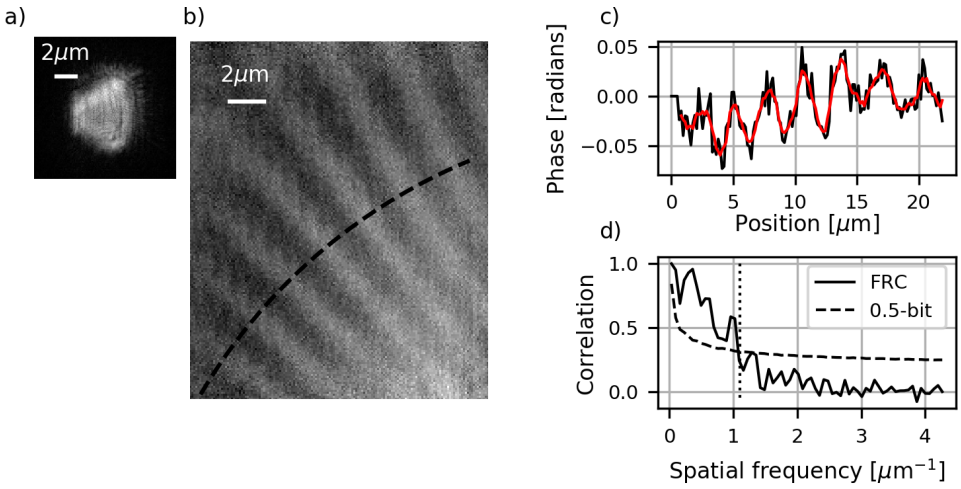

FIG. 2. The ptychography reconstruction. a) Modulus of the beam profile at the sample plane. b) Phase image of the Siemens star test target with a reconstructed pixel size of 116 nm. c) Line plot from the dashed black line in (b). The raw data is represented by the solid black line and the 10 pixel moving average is represented by the solid red line. d) Fourier ring correlation of the two split exposure reconstructions showing 1.08 µm^{-1} spatial frequency (corresponding to 930 nm).

Discussion and summary

Performing lab-based X-ray ptychography has required advances in lab-sources [20] and detector technologies [19]. The high brilliance of the LMJ has provided the coherent flux required for the ptychography technique. The hyperspectral detector has been required to characterise spectrally the source and assess the temporal coherence.

Our analysis of the results suggests that the experiment was limited by the photon statistics and point-to-point stability of the source. The effect of the latter was mitigated via the reconstruction algorithm that modelled the source shift and direction. The use of different or additional optical components for focussing the X-ray beam to the sample could help to better harness the coherent flux, increasing the photon statistics and reducing the sensitivity to long term source instabilities.

We have demonstrated that it is possible to perform X-ray ptychography with a LMJ source and have shown how to perform ptychography in a laboratory setting, releasing to the laboratory environment a technique otherwise confined to synchrotron facilities. The experimental breakthrough achieved with a LMJ is a first step toward expanding X-ray ptychography to other bright compact light sources: from inverse Compton scattering [24],

to laser-plasma based [25] and compact storage rings [26].

METHODS

Experimental configuration

X-ray source The X-ray beam is generated using a JXS-D2-001 liquid metal-jet laboratory source modified to a higher power performance (Excillum AB, Kista, Sweden) with Gallium as anode material. The focal spot size of the source can be varied within a relatively wide range between 5 µm and more than 50 µm, by tuning the projection of the electron beam on the Gallium jet stream with a set of electromagnetic lenses. For this experiment, the focal spot size was set to a nominal value of 5 µm. A three-dimensional single reflection multi-layered ellipsoidal mirror (FOX3D 11-600 Ga, Xenocs, Grenoble, France) is used to focus the X-ray beam. The centre of the mirror is located 11 cm downstream of the X-ray source, coinciding with the first mirror focus. The resulting beam is slightly converging, with the second mirror focus located approximately 5.2 m downstream of the mirror. Due to the chromatic behaviour of the mirror reflectivity, the mirror also acts as a spectral band-pass filter, enhancing the relative intensity of the 9.25 keV K-alpha emission line of Gallium by drastically reducing the Bremsstrahlung continuum spectrum.

Scanning system The portable ptycho-scope end-station developed at the I13-1 branch-line of the Diamond Light Source was used for positioning the sample and the pinhole (Figure 1). The ptycho-scope consists of two 3-axis SLC2430 piezo stages (SmarActs GmbH, Oldenburg, Germany), one for the pinhole and one for the sample. The stages are controlled with a python data collection software connected to an MCS control box over an RS232 protocol. The software scans the position point-by-point, triggers the detector through a USB-BNC connection and uses the detector ready status for synchronising the motion with the detector readout and beam status.

The instrument was set up with a 5 µm diameter, 50 µm thick, tungsten pinhole placed 4 m from the source. During the experiment, a flux through the pinhole of $\sim 5 \times 10^3\,\mathrm{photons\,s^{-1}}$ was measured. The sample was placed 1 cm downstream of the pinhole and scanned in the plane perpendicular to the optical axis of the beam on a square grid of 20×20 steps with step size of 1 µm, following a snake-like trajectory.

X-ray detector The pnCCD based Color X-ray Camera (SLcam) [27] was used to measure the diffraction patterns. The detector has a physical pixel pitch of 48 µm, and an active area of 264 × 264 pixels. The system was operated at a readout speed of 400 fps. The in-house developed software SpeXiDAQ [28] was used for camera control and readout as well as raw data processing. The energy resolution of the SLcam is approximately 144 eV FWHM at the Mn K-alpha peak and the centre of mass accuracy is better than 10 eV [29]. The detector was placed downstream of the sample at 9.4 m from the source. Vacuum pipes were placed between the sample and the detector as well as between the mirror and the pinhole to reduce the air absorption and scattering. The detector exposure at each point was 140 s, with a single scan taking 16 hours in total.

Sample The Siemens star is a 500 nm thick gold structure deposited on a silicon nitride membrane with an outer spoke separation of 4 µm and an inner spoke separation of 50 nm. An area of 400 μm^2 was scanned during the experiment.

Data processing

Detector frame processing The SLcam captures raw frames containing only a few photon events per frame. The raw frames are subsequently pre-processed into diffractograms for the ptychography reconstruction, using a cluster-finding algorithm and subsequent rebinning of the retrieved events into a 3D datacube (two spatial dimensions and one spectral dimension). Due to this processing method, charge sharing effects do not deteriorate the spectral response and sub-pixel accuracy can be achieved [30]. Using SpeXiDAQ [28], the raw frames are stored and afterward processed and split by time or energy into different datasets. The time-based splitting was used for assessing the spatial resolution (see post-processing section below), the energy-based splitting for investigating the spectral properties. The spectrum has been generated by integrating the photon counts in each of the 5 eV energy bin datasets. The spectrum recorded is shown in Figure 3: the escape peak of the K-alpha line in the Silicon bulk and the double and triple photon pile-up of the K-alpha are visible, beside the main Ga K-alpha and K-beta peaks. The source spectrum has been retrieved by adding the counts of the escape peak, those of the double pile-up (×2) and of the triple pile-up (×3) to the K-alpha peak. The energy bandwidth was investigated and matched to the resolution achievable from the experimental conditions (flux and geometry). The data shown in Figure 2 was produced

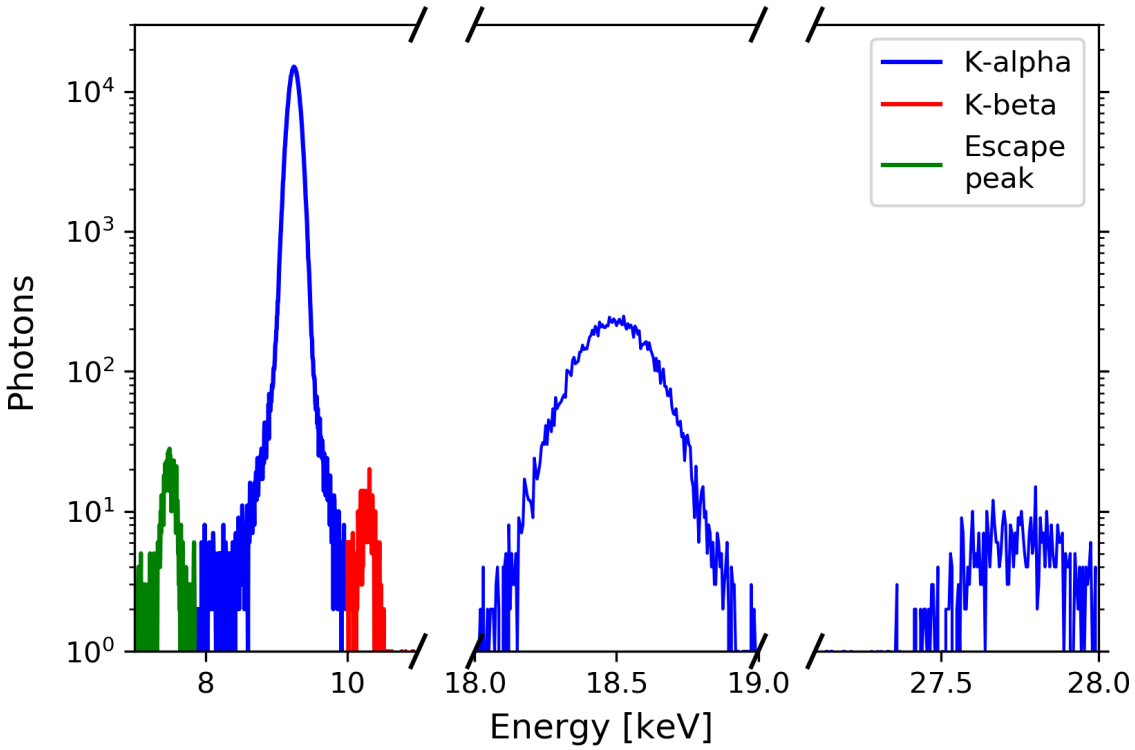

FIG. 3. The X-ray source spectrum as recorded with the SLcam. The Ga K-alpha peak (9.25 keV) along with the double pile-up (18.5 keV) and triple pile-up peaks (27.75 keV) are shown in blue. The K-alpha escape peak in Si (7.51 keV) is shown in green and the K-beta (10.26 keV) is shown in red.

using a single output bin ranging from 8.75 keV to 9.75 keV.

Image reconstruction

The image reconstruction process takes a model of the experiment, including knowledge of the illumination conditions and scanning coordinates along with the recorded intensity measurements, and applies physical constraints in order to solve for the unknown sample. Here, the illumination was initially modelled as a convergent beam of 1 mrad full angle and a defocus of 10 mm. The convergence angle is calculated from the beam on the detector, and the defocus was chosen to produce a 5 µm spot creating a balance between the true focal distance of the mirror and the beam width imposed by the pinhole. The scanning

coordinates are taken from the requested values of the SmarAct motors.

The ptychographic data were processed with 500 iterations of the ePIE operator [12] available in PtyREX [22]. The reconstruction algorithm is capable of dealing with source instability, experimental errors and signal degradation due to noise and decoherence. The beam intensity was monitored during the acquisition by integrating the flux received on the detector. The intensity variations, shown in Figure 4(a), are a manifestation of the source instabilities. The source appears to fluctuate across the first 100 positions, with a significant sudden drop in intensity at position 131 of the scan. Scan positions 131 and 132 were removed from the data prior to the reconstruction (see Figure4). The source fluctuations translate into point-to-point instabilities at the sample plane and correspond to either a translation, a tilt, or a combination of the two in the beam profile. PtyREX employs a scan correction built on the annealing method of Maiden et al. [31], but is extended to also accommodate angular variations in the incident beam within the same update step. The position and tilt correction applied during the reconstruction are shown Figure 4(b).

The impact of the source properties, detector readout, and beam-sample positions on the reconstruction quality, was investigated. In order to understand the effects of each element and to extract the maximum image quality, a multidimensional parameter sweep was performed on the HPC cluster of Diamond Light Source. The parameters included were the number of source states [32, 33], number of scan correction trials [31], detector threshold levels, and the bandwidth of the diffraction data. Each parameter permutation was executed on the split and complete exposure data, allowing for a quantitative comparison of the resolution.

Post-processing To quantify the attained resolution, the acquired dataset was divided (in time) into two half datasets to perform a Fourier Ring Correlation (FRC) analysis. The correlation between the two half datasets was compared to a half-bit information threshold, using an implementation based on van Heel et al. [34]. The splitting was done by alternately assigning a camera time-frame series to the odd or even dataset. Since the frame interval is very short (2.5 ms) compared to the expected timescale of source fluctuations, these half datasets can be considered to be statistically independent measurements of the same source-object-camera system, including its fluctuations. The obtained FRC curve is shown in Figure 2(d), as well as the half-bit threshold curve used to determine the attained resolution. The crossover point of the two curves lies at 1.08 μm^{-1}, corresponding to a resolution of

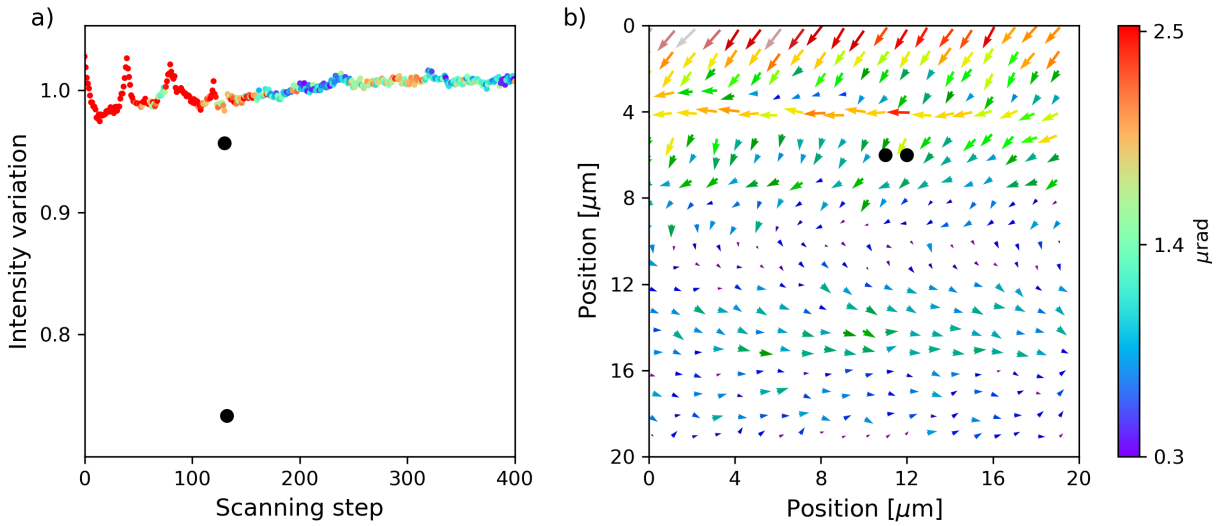

FIG. 4. Source and illumination stability. a) Fluctuation of total intensity measured by integrating the total flux on the detector during the scan. The value is normalised by the mean value. b) Beam position and tilt correction as recovered during the PtyREX reconstruction. The origin of the arrow represents the re-calculated position, the direction of the arrow represents the direction of the tilt correction, and the length of the arrow is proportional to the modulus of the angular tilt. The colormap of both (a) and (b) represents the modulus of the angular tilt at each scan position, highlighting the correlation between intensity fluctuations and angular tilt corrections. The two points removed during the reconstruction are marked as black dots both in (a) and (b).

930 nm. The correlation in Fourier-space was determined over 65 rings. For completeness, a line profile is provided, taken along an arc centred at the middle of the Siemens star.

ACKNOWLEDGEMENTS

O.O.M thanks EPSRC for the capital equipment grant (EP/M028437/1) to purchase the laboratory-based Xenocs Xeuss 2.0/Excillum SAXS beamline used for the data collection.

The Research Foundation - Flanders (FWO) is acknowledged for the financial support to this work (Grant number G0A0417N).

The authors acknowledge Dr. Christian David for the design and production of the Siemens star test pattern.

CONTRIBUTION

The experiment was conceived by D.J.B. and S.C. and was conducted by D.J.B., S.C., F.V.A., S.V., O.O.M and A.J.P.. The portable ptycho-scope was developed by S.C., D.J.B and C.R.. The raw data were processed by F.V.A., S.V and M.N.B.. Reconstruction and analysis was performed by D.J.B., S.V. and S.C.. The manuscript was written by D.J.B., S.C., M.N.B., S.V. and F.V.A.. All the authors reviewed the manuscript.

[1] H. M. L. Faulkner and J. M. Rodenburg, Movable aperture lensless transmission microscopy: A novel phase retrieval algorithm, Physical Review Letters **2**, 023903 (2004).

[2] J. M. Rodenburg, A. C. Hurst, A. G. Cullis, B. R. Dobson, F. Pfeiffer, O. Bunk, C. David, K. Jefimovs, and I. Johnson, Hard-x-ray lensless imaging of extended objects, Physical Review Letters **3** (2007).

[3] M. Dierolf, A. Menzel, P. Thibault, P. Schneider, C. M. Kewish, R. Wepf, O. Bunk, and F. Pfeiffer, Ptychographic x-ray computed tomography at the nanoscale, Nature **7314**, 436 (2010).

[4] Y. Takahashi, A. Suzuki, N. Zettsu, Y. Kohmura, Y. Senba, H. Ohashi, K. Yamauchi, and T. Ishikawa, Towards high-resolution ptychographic x-ray diffraction microscopy, Physical Review B - Condensed Matter and Materials Physics **21** (2011).

[5] J. Vila-Comamala, A. Diaz, M. Guizar-Sicairos, A. Mantion, C. M. Kewish, A. Menzel, O. Bunk, and C. David, Characterization of high-resolution diffractive x-ray optics by ptychographic coherent diffractive imaging, Optics Express **22**, 21333 (2011).

[6] A. Schropp, R. Hoppe, J. Patommel, D. Samberg, F. Seiboth, S. Stephan, G. Wellenreuther, G. Falkenberg, and C. G. Schroer, Hard x-ray scanning microscopy with coherent radiation: Beyond the resolution of conventional x-ray microscopes, Applied Physics Letter **100**, 10.1063/1.4729942 (2012).

[7] M. Holler, A. Diaz, M. Guizar-Sicairos, P. Karvinen, E. Färm, E. Härkönen, M. Ritala, A. Menzel, J. Raabe, and O. Bunk, X-ray ptychographic computed tomography at 16 nm isotropic 3d resolution, Scientific Reports **1**, 3857 (2014).

[8] A. Schropp, R. Hoppe, V. Meier, J. Patommel, F. Seiboth, H. J. Lee, B. Nagler, E. C. Galtier, B. Arnold, U. Zastrau, J. B. Hastings, D. Nilsson, F. Uhlén, U. Vogt, H. M. Hertz, and C. G. Schroer, Full spatial characterization of a nanofocused x-ray free-electron laser beam by ptychographic imaging, Scientific Reports **1**, 1633 (2013).

[9] D. J. Batey, S. Cipiccia, F. Van Assche, S. Vanheule, J. Vanmechelen, M. N. Boone, and C. Rau, Spectroscopic imaging with single acquisition ptychography and a hyperspectral detector, Scientific Reports **9** (2019).

[10] S. Marchesini, H. Krishnan, B. J. Daurer, D. A. Shapiro, T. Perciano, J. A. Sethian, and F. R. N. C. Maia, Sharp: a distributed gpu-based ptychographic solver, Journal of Applied Crystallography **4**, 1245 (2016).

[11] B. Enders and P. Thibault, A computational framework for ptychographic reconstructions, Proceeding of the Royal Society A 10.1098/rspa.2016.0640 (2016).

[12] A. M. Maiden and J. M. Rodenburg, An improved ptychographical phase retrieval algorithm for diffractive imaging, Ultramicroscopy **10**, 1256 (2009).

[13] M. Guizar-Sicairos and J. R. Fienup, Phase retrieval with transverse translation diversity: a nonlinear optimization approach, Optics Express **16**, 7264 (2008).

[14] K. Wakonig, H.-C. Stadler, M. Odstrcil, E. H. R. Tsai, A. Diaz, M. Holler, I. Usov, J. Raabe, A. Menzel, and M. Guizar-Sicairos, Ptychoshelves, a versatile high-level framework for high-performance analysis of ptychographic datathis article will form part of a virtual special issue of the journal on ptychography software and technical developments, Journal of Applied Crystallography **2**, 574 (2020).

[15] M. Wansleben, C. Zech, C. Streeck, J. Weser, C. Genzel, B. Beckhoff, and R. Mainz, Photon flux determination of a liquid-metal jet x-ray source by means of photon scattering, arXiv 10.1039/C9JA00127A (2019).

[16] M. J. Derry, O. O. Mykhaylyk, A. J. Ryan, and S. P. Armes, Thermoreversible crystallization-driven aggregation of diblock copolymer nanoparticles in mineral oil, Chemical Science **17**, 4071 (2018).

[17] H. M. Thirimanne, K. D. G. I. Jayawardena, A. J. Parnell, R. M. I. Bandara, A. Karalasingam, S. Pani, J. E. Huerdler, D. G. Lidzey, S. F. Tedde, A. Nisbet, C. A. Mills, and S. R. P. Silva, High sensitivity organic inorganic hybrid x-ray detectors with direct transduction and broadband response, Nature Communications **9** (2018).

[18] A. Bjeoumikhov, G. Buzanich, N. Langhoff, I. Ordavo, M. Radtke, U. Reinholz, H. Riesemeier, O. Scharf, H. Soltau, and R. Wedell, The SLcam: a full-field energy dispersive x-ray camera, Journal of Instrumentation **7** (11), C11008.

[19] O. Scharf, S. Ihle, I. Ordavo, V. Arkadiev, A. Bjeoumikhov, S. Bjeoumikhova, G. Buzanich, R. Gubzhokov, A. Gunther, R. Hartmann, M. Kuhbacher, M. Lang, N. Langhoff, A. Liebel, M. Radtke, U. Reinholz, H. Riesemeier, H. Soltau, L. Struder, A. F. Thunemann, and R. Wedell, Compact pnccd-based x-ray camera with high spatial and energy resolution: A color x-ray camera, Analytical Chemistry **7**, 2532 (2011).

[20] https://www.excillum.com/applications/.

[21] M. Otendal, T. Tuohimaa, U. Vogt, and H. M. Hertz, A 9 kev electron-impact liquid-gallium-jet x-ray source, Review of Scientific Instruments **79**, 016102 (2008).

[22] D. J. Batey, *Ptychographic Imaging of Mixed States*, Thesis, University of Sheffield (2014).

[23] J. C. H. Spence, U. Weierstall, and M. Howells, Coherence and sampling requirements for diffractive imaging, Ultramicroscopy **2**, 149 (2004).

[24] B. Gunther, R. Gradl, C. Jud, E. Eggl, J. Huang, S. Kulpe, K. Achterhold, B. Gleich, M. Dierolf, and F. Pfeiffer, The versatile x-ray beamline of the munich compact light source: design, instrumentation and applications, Journal of Synchrotron Radiation **5**, 1395 (2020).

[25] S. Cipiccia, M. R. Islam, B. Ersfeld, R. P. Shanks, E. Brunetti, G. Vieux, X. Yang, R. C. Issac, S. M. Wiggins, G. H. Welsh, M.-P. Anania, D. Maneuski, R. Montgomery, G. Smith, M. Hoek, D. J. Hamilton, N. R. C. Lemos, D. Symes, P. P. Rajeev, V. O. Shea, J. M. Dias, and D. A. Jaroszynski, Gamma-rays from harmonically resonant betatron oscillations in a plasma wake, Nature Physics **11**, 867 (2011).

[26] G. P. Williams, Compact electron storage rings, Nuclear Instruments and Methods in Physics Research Section A: Accelerators, Spectrometers, Detectors and Associated Equipment **1**, 59 (1988).

[27] I. Ordavo, S. Ihle, V. Arkadiev, O. Scharf, H. Soltau, A. Bjeoumikhov, S. Bjeoumikhova, G. Buzanich, R. Gubzhokov, A. Günther, R. Hartmann, P. Holl, N. Kimmel, M. Kühbacher, M. Lang, N. Langhoff, A. Liebel, M. Radtke, U. Reinholz, H. Riesemeier, G. Schaller, F. Schopper, L. Strüder, C. Thamm, and R. Wedell, A new pnccd-based color x-ray camera for fast spatial and energy-resolved measurements, Nuclear Instruments and Methods in Physics Research Section A: Accelerators, Spectrometers, Detectors and Associated Equipment **1**, 250

(2011).

[28] F. Van Assche, S. Vanheule, L. Van Hoorebeke, and M. N. Boone, The spectral x-ray imaging data acquisition (spexidaq) framework, Sensors **2**, 563 (2021).

[29] F. Van Assche, S. Vanheule, S. Cipiccia, L. Vincze, L. Van Hoorebeke, and M. N. Boone, Implementation of a hyperspectral x-ray camera control and processing software chain, J. Instrum **13**, C11015 (2018).

[30] S. H. Nowak, A. Bjeoumikhov, J. von Borany, J. Buchriegler, F. Munnik, M. Petric, M. Radtke, A. D. Renno, U. Reinholz, O. Scharf, and R. Wedell, Sub-pixel resolution with a color x-ray camera, Journal of Analytical Atomic Spectrometry **9**, 1890 (2015).

[31] A. M. Maiden, M. J. Humphry, M. C. Sarahan, B. Kraus, and J. M. Rodenburg, An annealing algorithm to correct positioning errors in ptychography, Ultramicroscopy **120**, 64 (2012).

[32] D. J. Batey, D. Claus, and J. Rodenburg, Information multiplexing in ptychography, Ultramicroscopy **138C**, 13 (2013).

[33] P. Thibault and A. Menzel, Reconstructing state mixtures from diffraction measurements, Nature **7435**, 68 (2013).

[34] M. van Heel and M. Schatz, Fourier shell correlation threshold criteria, Journal of structural biology **3**, 250 (2005).